Transparent nanoplates of Diaqua oxalato strontium(II) for adsorption uptake of Eriochrome Black T in aqueous solution

Amr Mohamed Nassar*, Nasser Fahad Alotaibi

Chemistry Department, College of Science, Jouf University, Sakaka, Saudi Arabia, Tel. 00966555978016; emails: amnassar@ju.edu.sa (A.M. Nassar), nfalotaibi@ju.edu.sa (N.F. Alotaibi)

ABSTRACT

Transparent nanoplates of Diaqua oxalato strontium(II) [$Sr(C_2O_4)(H_2O)_2$], SrOx-NPs, were prepared and employed as adsorbents in an aqueous solution of azodye Eriochrome Black T (EBT). X-ray diffraction, scanning electron microscopy, transmission electron microscopy, and Fourier-transform infrared spectra were used to investigate the structure and morphology of SrOx-NPs. To identify the optimal conditions for EBT adsorption by SrOx-NPs, studies were carried out at initial dye concentrations, adsorbent doses, contact reaction time, pH, and temperature. The investigations revealed that the best conditions for EBT adsorption on the SrOx-NPs surface were natural pH (pH = 6), dose concentration of 0.5 g L^{-1}, initial dye concentration of 40 mg L^{-1}, and temperature 25°C. The equilibrium uptake increased as the amount of SrOx-NPs increased. Fitting the findings of the adsorption studies to Langmuir and Freundlich isotherms were used to examine them. The best fit is provided by the Freundlich model, which has an adsorption capacity of 63 mg g^{-1} and a correlation value of R^2 = 0.9837%. The kinetic mechanism of adsorption was investigated using pseudo-first-order and pseudo-second-order kinetic models. The experimental data matches well with a pseudo-second-order kinetic model, with a correlation value of 0.96. The adsorption process's thermodynamic parameters were also determined.

Keywords: Diaqua oxalato strontium(II); Nanoplates; Adsorption; Aqueous; Eriochrome Black T

1. Introduction

Water pollution is one of the major issues that many countries face [1]. Dyes, phenols, metals, pesticides, viruses, and bacteria are amongst the pollutants found in wastewater [2]. Due to the global water shortage problem, water purification from harmful pollutants is an important aspect of environmental management. Azo dyes are a type of organic pollutant with the –N=N– functional group as a chromophore in their chemical structure [3]. Although azo dyes are used in a wide range of industries, including textiles, leather, chemical and biological laboratories, plastic, paint, and the food industry, they are toxic to humans and cause serious diseases [4]. Azo dyes are stubborn chemicals that remain stable in the presence of air, light, and temperature. Since azo dyes are very toxic, dangerous and carcinogenic [5], their removal from effluents is a major concern.

Eriochrome Black T (EBT) is an azo dye that is widely used in volumetric titration and industrial applications for complexometric estimation of metal ions [6]. The chemical formula/molecular weight of EBT is $C_{20}H_{12}N_3NaO_7S$/461.38, with a color index of 14,645 and a chromophore absorption band of max 530 nm [7]. EBT is classified as toxic to aquatic life with long lasting effects [8]. Traditional aerobic treatment and biological oxidative reactions do not decompose EBT. So, removing EBT from water is a hard process to handle.

---

* Corresponding author.

The adsorption process is one of several effective chemical and physical techniques used in wastewater purification. The adsorption process is widely used in comparison to other techniques because it is simple, effective, safe, easy to handle, low-cost, and capable of working at very low concentrations of pollutants removal [9]. Several adsorbents, such as zeolite [10], graphene [11], activated carbon [12], biochars [13], Fe_2O_3/grapheme oxide [14] and polymeric nanocomposite [15] have been studied for the removal of EBT from water.

A waste of bottom ash and de-oiled soya have been tested as adsorbents for removing a water–soluble azo dye. IR and DTA were used to characterize the adsorbents. The effects of pH, adsorbate dosage, and particle size on the adsorption process were performed using a batch adsorption approach. The Langmuir, Freundlich, Temkin, and Dubinin–Radushkevich isotherms were used to test the experimental results and their parameter constants were obtained. The thermodynamics reveal that the process is exothermic and spontaneous. According to the kinetic studies, the adsorption process follows first-order kinetics. Bottom ash and de-oiled soya were saturated at 89.9% and 94%, respectively, in a fixed-bed adsorption experiment, indicating that both adsorbents could be cost-effective [16].

Strontium oxalate, SrC_2O_4, is a compound that can exist in three states: anhydrous, neutral hydrated, and acidic [17]. The resulting form of strontium oxalate depends on the starting oxalate precipitant type; oxalic acid, sodium oxalate or ammonium oxalate; and reaction conditions such as temperature and pH [18]. Recently, $[Sr(C_2O_4)(H_2O)_2]$ was used as a Congo red adsorbent in water, with a removal percentage of 60.50% under studied conditions [19].

In this work, a new adsorbent, Diaqua oxalato strontium(II), is prepared and characterized. On the anionic hazardous dye Eriochrome Black T, the material's adsorption capacity was evaluated. To the best of our knowledge, the adsorption properties of Diaqua oxalato strontium(II) are innovative, and no attempt has been made to verify its batch adsorption capability for removing harmful dyes from wastewater.

2. Experimental

2.1. Materials

Strontium nitrate, hydrated oxalic acid, and EBT are Sigma-Aldrich chemicals (USA) and are used as received. A stock EBT solution of 100 mg L^{-1} concentration was prepared and serial dilutions were made for the required concentrations using bi-distilled water.

2.2. Preparation of Diaqua oxalato strontium(II) nanoplates; SrOx-NPs

In our previous work, SrOx-NPs were prepared according to a reported method. [19]. In 20 mL of water, $Sr(NO_3)_2$ (2.11 g, 0.01 mol) was dissolved. Then, a 20 mL solution of $(COOH)_2 \cdot 2H_2O$ (1.26 g, 0.01 mol) was mixed with the pervious solution. The mixture was heated at 75°C under stirring (100 rpm) at 75°C. After 1 h, the white precipitate formed was filtered (MF-Millipore TM Membrane Filter, 0.45 μm pore size). The precipitate was washed three times with hot water and kept to dry in the air at room temperature.

2.3. Structural and surface characterization of SrOx-NPs

The structure and morphology of SrOx-NPs were determined using X-ray diffraction (XRD; XRD-7000–Shimadzu), Fourier-transform infrared (FT-IR) spectra (FT-IR affinity-1S Shimadzu), scanning electron microscopy (SEM; JSM 6360 LA, Japan) and transmission electron microscopy (TEM; JEOL-JEM-1230 microscope).

2.4. Adsorption studies

Adsorption experiments were carried out to study the effects of different parameters (adsorbent masses, initial dye concentrations, contact time, pH and temperature) on the adsorption process. In this experiment, 100 mL of EBT (10–100) mg/L solution was mixed with various doses of adsorbent in a 250 mL beaker and stirred in the dark for 20 min at room temperature (20°C–45°C) of pH is carried out using 0.1 M NaOH and HCl. After agitation, the mixture was centrifuged for 5 min. Then the concentration of the dye in the upper fluid was used by a UV-Vis spectrophotometer set at a λ, 530 nm. Adsorption capacity at equilibrium (q_e, mg g^{-1}) and percentage of dye removal (%) were calculated from Eqs. (1) and (2), [20], respectively.

$$q_e = \frac{C_0 - C_e}{m} \times V \tag{1}$$

$$R\% = \frac{C_0 - C_e}{C_0} \times 100 \tag{2}$$

where C_0 is the initial EBT concentration (mg L^{-1}), C_e is the concentration of EBT at equilibrium (mg L^{-1}), V is the applied volume of dye (L), and m is the mass of the adsorbent (g).

3. Results and discussion

3.1. Characterization of SrOx-NPs

3.1.1. XRD patterns

The resultant XRD patterns of Diaqua oxalato strontium(II), as shown in Fig. 1, were similar to the tetragonal crystalline structure of hydrated strontium oxalate obtained from XRD analysis, as reported by Chen et al. [21]. The sharp peaks indicate high crystanallity, which agrees well with SEM and TEM images. The average crystalline size was obtained from the Debye–Scherrer equation [22], Eq. (3).

$$D = \frac{0.9 \cdot \lambda}{\beta \cdot \cos\theta} \tag{3}$$

where D is average crystalline size, λ is wavelength (1.5418 Å), β is half maximum width and θ is diffraction angle. The calculated D was 16.58 nm, indicating the crystal size of the prepared material is within the nanoscale.
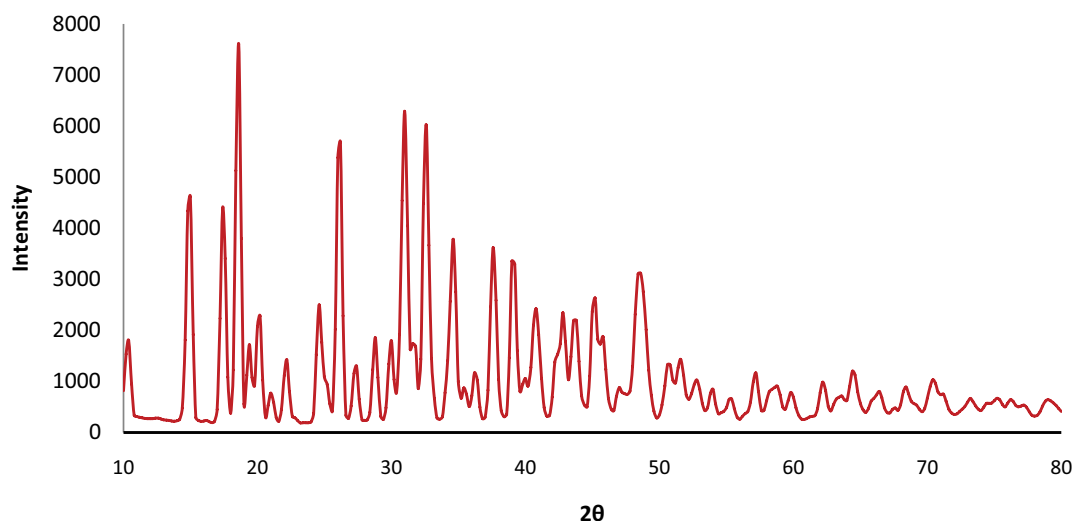
Fig. 1. XRD pattern of [SrC$_2$O$_4$·2H$_2$O].

3.1.2. FT-IR spectra

FT-IR spectra of the SrOx-NPs adsorbent before and after adsorption of EBT and EBT are shown in Fig. 2. As displayed, the spectrum of SrOx-NPs exhibits bands at 3,350; 1,703 and 1,640 cm^{-1} characteristics of H$_2$O stretching, –COO stretching, and H$_2$O bending vibrations, respectively [23,24]. The reaction of EBT with SrOx-NPs is confirmed by comparing the spectra of SrOx-NPs and EBT with that of EBT@SrOx-NPs, which displayed the weakness of the band at 3,350 and 1,703 cm^{-1} indicating the involvement of H$_2$O and –COO in hydrogen bonding with EBT. Also, the broadened band in the EBT spectrum at 3,390–3,458 cm^{-1}, which is attributed to the stretching of –OH groups is weakened in the spectrum of EBT@SrOx-NPs, indicating the participation of –OH groups in hydrogen bonding with the adsorbent [25]. From these findings, we can conclude that the adsorption of EBT on SrOx-NPs takes place via hydrogen bonding between the adsorbate and the adsorbent [26,27].

3.1.3. Morphological studies

Fig. 3 shows the morphology of the sample and shows that there are different contrast spots that appear in SEM images a and b. These spots could be attributed to the different densities of material at these places. Clearly, TEM images showed that these spots appeared on images c and b with different densities, which was attributed to the formation of porous, transparent, synthesized Diaqua oxalato strontium(II). Therefore, the prepared compound can be characterized as a transparent and porous material according to SEM and TEM results.

3.2. Batch adsorption studies

3.2.1. Effect of pH

The effect of solution pH 2, 4, 6, 8, and 10 on the adsorption percentage of EBT was studied by mixing 50 mg of SrOx-NPs with 100 mL of EBT solution concentration of 40 mg L^{-1} at room temperature. It is noticeable during the addition of HCl or NaOH that it reveals disintegration of some adsorbents. As shown in Fig. 4, the best pH value for EBT adsorption is the natural pH 6. Decreasing pH values leads to a decrease in adsorption removal. Also, as pH values increase, the adsorption efficiencies decrease. This may be associated with the decomposition of the adsorbent during the addition of HCl or NaOH and the conversion of water insoluble SrOx-NPs into soluble Sr^{2+} + Cl$^-$ or Sr^{2+} + OH$^-$, respectively.

3.2.2. Effect of contact time

To determine the equilibrium time for EBT adsorption, the effect of contact time (0–30 min) of adsorption of EBT (40 mg L^{-1}) on the SrOx-NPs surface (50 mg) was investigated at ambient temperature (20°C). Fig. 5 shows the plot of applied time vs. removal efficiency at a definite time (q_t). As shown, the adsorption efficiency increases with contact time increasing from 5–20 min followed by almost constant efficiency value at 25 min which reveals that the adsorption reached equilibrium within 20 min. This is due to after equilibrium all active sites on adsorbent surface are blocked by dye molecules and no more sites are available for binding [28].

3.2.3. Effect of initial dye concentration

The adsorption efficiency of EBT was scrutinized with variation of its initial concentration (10–70 mg L^{-1}) at ambient temperature, time (20 min), SrOx-NPs dose of 50 mg, and natural pH. The results are shown in Fig. 6. The adsorption efficiency was raised with a rise in dye concentration from 10–40 mg L^{-1}. It refers to the available binding sites on the SrOx-NPs surface that are able to compete with dye molecules in the solution until this concentration. At an initial 50 mg L^{-1} concentration, the adsorption efficiency was almost the same as at an initial
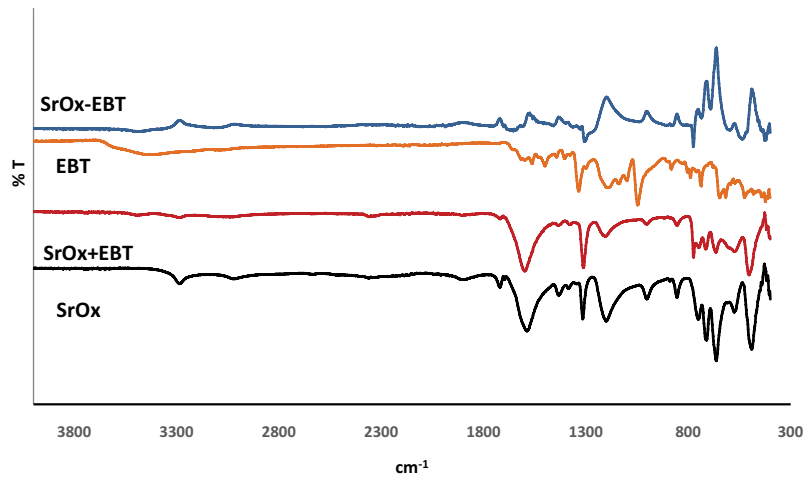
Fig. 2. FT-IR spectra of [SrC$_2$O$_4$·2H$_2$O] before and after EBT adsorption.
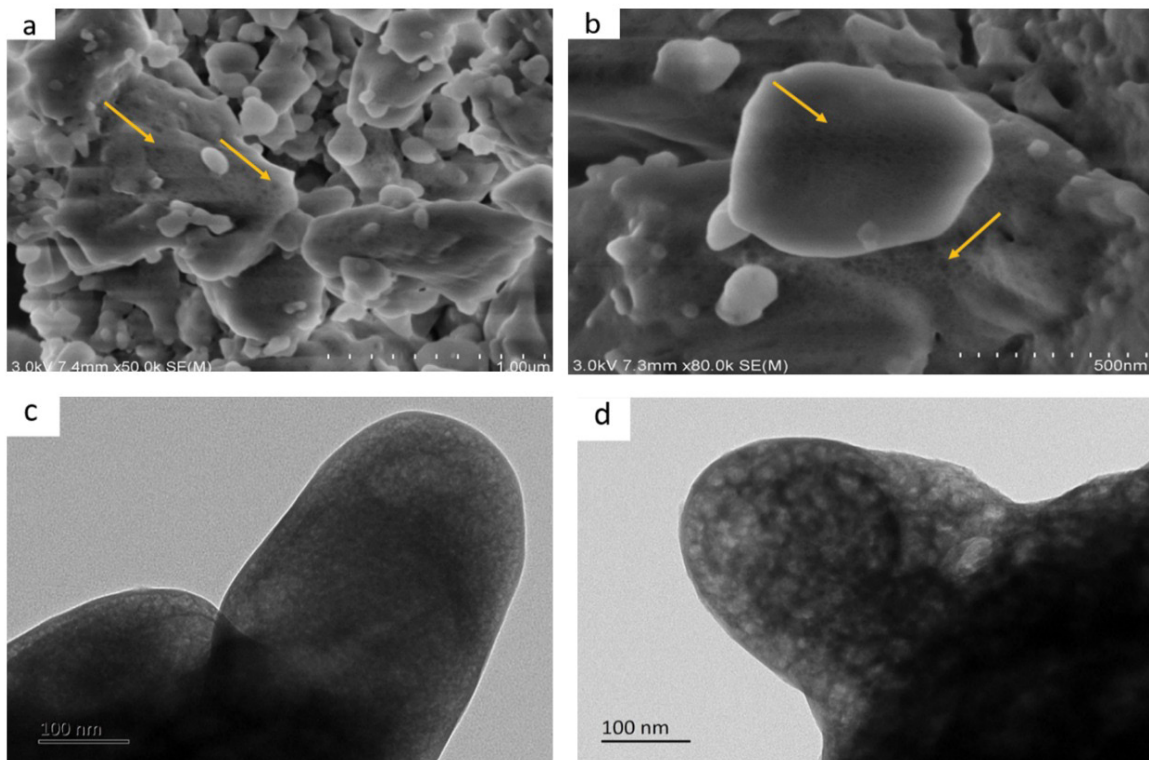
Fig. 3. SEM images (a, b) and TEM images (c, d) of [SrC$_2$O$_4$·2H$_2$O].

concentration of 40 mg L^{-1}. Then, the rise in concentrations from 60 to 70 mg L^{-1} was occupied by the rise in adsorption efficiency. This is perhaps owing to the activation of covered sites in the adsorbent surface with the increase in EBT molecules [29].

3.2.4. Effect of variation of adsorbent amount

The effect of the amount of SrOx-NPs on the adsorption process of EBT (100 mL, 40 mg L^{-1}) was studied with a variation of doses in the range of 10–110 mg for 20 min at natural pH and room temperature. By increasing the SrOx-NPs dose from 10–50 mg, the adsorption percentage also increases until it reaches its saturation point at dose 50 mg. After this amount, there was no change in removal percentage by increasing the adsorbent dose from 60–110 mg. This is attributed to the increasing dose also increasing the surface active sites fitted for molecular adsorption and reaching saturation at 50 mg [30]. The adsorbent concentration of 50 mg is adequate for the adsorption of EBT molecules.
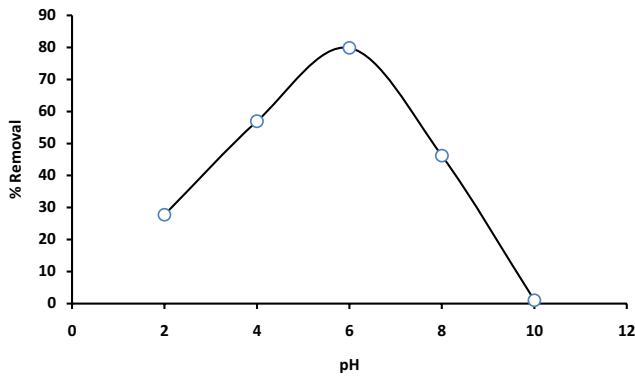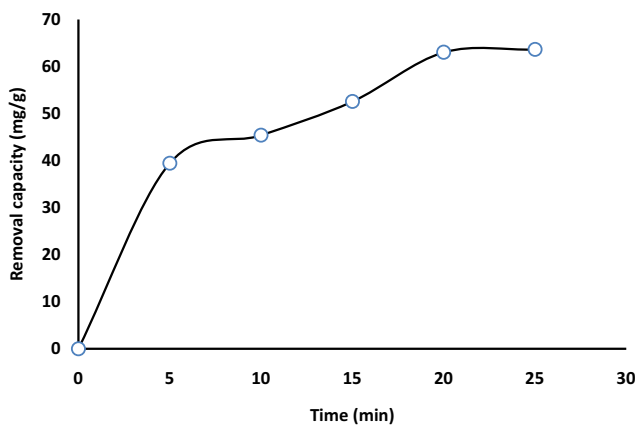
Fig. 4. Effect of pH on adsorption removal of EBT.
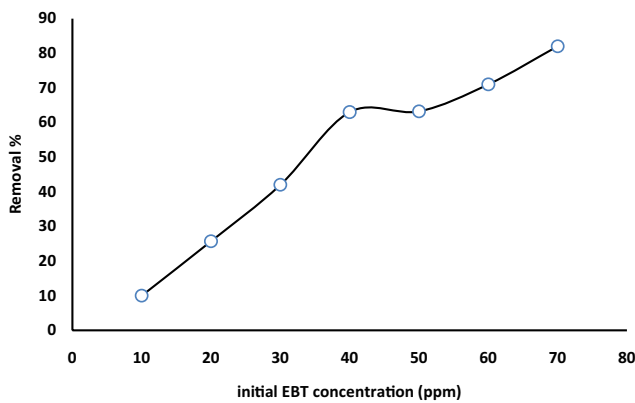

Fig. 5. Effect of contact time on adsorption capacity.

Fig. 6. Effect of initial EBT concentration on adsorption capacity.

3.2.5. Adsorption isotherms

The interaction and adsorption system of EBT with SrOx-NPs is described by an adsorption isotherm. The adsorption results were fixed with linear equations of the linear Langmuir and Freundlich models, Eqs. (4) and (5), respectively [31].

$$\frac{1}{q_e} = \frac{1}{k_1 q_m}\frac{1}{C_e} + \frac{1}{q_m} \qquad (4)$$

where q_e (mg g^{-1}) is the adsorption capacity of dye at equilibrium, q_m (mg g^{-1}) is the maximum adsorption capacity, C_e (mg L^{-1}) is the concentration of dye at equilibrium, and k_1 is the Langmuir constant.

$$\log q_e = \log K_f + \frac{1}{n}\log C_e \qquad (5)$$

where q_e (mg g^{-1}) is the adsorption capacity of dye at equilibrium, C_e (mg L^{-1}) is the concentration of dye at equilibrium, K_f is Freundlich constant (L mg^{-1}) related to adsorption capacity and $1/n$ is adsorption intensity.

As shown in Fig. 7a, Langmuir isotherm model is not fitted with adsorption of EBT and SrOx-NPs with calculated value of $R^2 = 0.7106$ indicating the non-homogeneous nature of SrOx-NPs surface [32]. By applying Freundlich isothermal model, plot of lnq_e vs. lnC_e, Fig. 7b exhibits an acceptable linearity straight line. The value of $R^2 = 0.9813$ shows well agreement with Freundlich model indicates the adsorption of EBT molecules on the heterogeneous surface of SrOx-NPs via hydrogen or chemical bonds [33].

3.2.6. Adsorption kinetics

To determine the kinetic mechanism of EBT adsorption from aqueous solution by SrOx-NPs, kinetic models of pseudo-first-order and pseudo-second-order were studied in this work. As shown in Fig. 5, equilibrium was reached in 20 min. The linear equations for pseudo-first-order and pseudo-second-order are given in Eqs. (6) and (7), [34], respectively.

$$\ln\left(q_e - q_t\right) = \ln q_e - k_1 t \qquad (6)$$

$$\frac{t}{q_t} = \frac{1}{k_2 q_2 e} + \frac{t}{q_e} \qquad (7)$$

where k_1 (min^{-1}) and k_2 (g mg^{-1} min^{-1}) are rate constants of pseudo-first-order and pseudo-second-order, respectively. q_t and q_e are the capacities of adsorption at time t and equilibrium, respectively.

The correlation coefficient of the pseudo-first-order model ($R^2 = 0.80$), which is not well fitted with adsorption experimental data, Fig. 8a. On the other hand, the correlation coefficient of the pseudo-second-order model ($R^2 = 0.96$), Fig. 8b. This finding confirms that the kinetics data fits best with a pseudo-second-order kinetics model, Table 1.

3.2.7. Thermodynamic studies

The adsorption thermodynamic equilibrium constant K was determined as Eq. (8) [35].

$$K = \frac{q_e}{C_e} \qquad (8)$$

where q_e is the capacity adsorption of EBT and C_e is the equilibrium EBT concentration in solution (mol L^{-1}). The standard free energy change ($\Delta G°$) (kJ mol^{-1}), enthalpy ($\Delta H°$) (kJ mol^{-1}) and entropy change ($\Delta S°$) (kJ mol^{-1}) for

Table 1
Adsorption isotherm and kinetic model

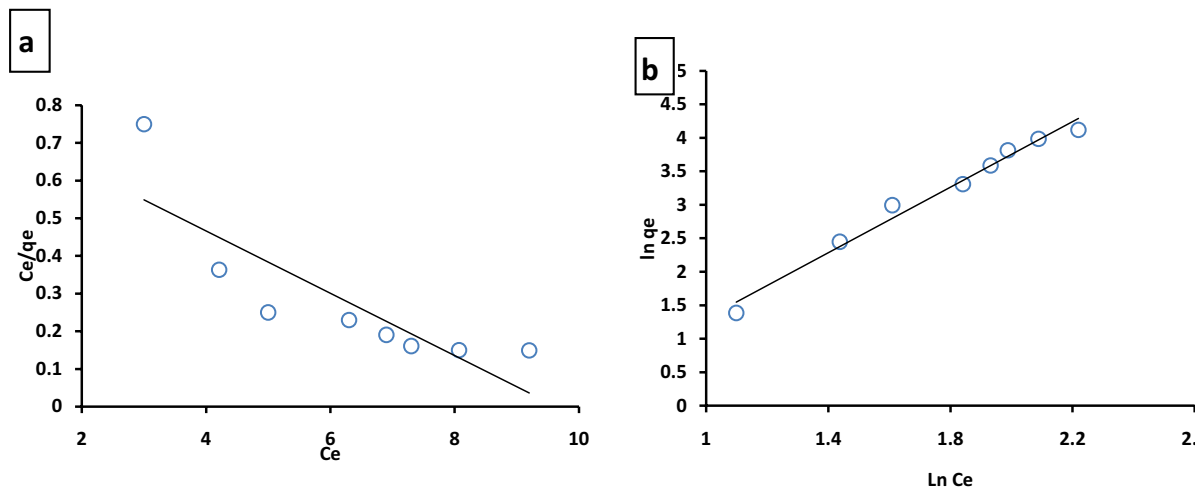| Model	Formula	Value	Equation	References
Langmuir isotherm model	$\dfrac{1}{q_e} = \dfrac{1}{k_1 q_m}\dfrac{1}{C_e} + \dfrac{1}{q_m}$	$R^2 = 0.7106$	(4)	[31]
Freundlich isotherm model	$\log q_e = \log K_f + \dfrac{1}{n}\log C_e$	$R^2 = 0.9813$	(5)	[31]
Pseudo-first-order kinetic model	$\ln(q_e - q_t) = \ln q_e - k_1 t$	$R^2 = 0.80$	(6)	[34]
Pseudo-second-order kinetic model	$\dfrac{t}{q_t} = \dfrac{1}{k_2 q_2 e} + \dfrac{t}{q_e}$	$R^2 = 0.96$	(7)	[34]

Fig. 7. Plots of Langmuir (a) and Freundlich (b) isothermal models for the adsorption of EBT with SrOx-NPs.

the adsorption reaction were calculated using Eqs. (9) and (10) [36]:

$$\Delta G = -RT \ln K \tag{9}$$

where R is the gas constant (8.314 J mol^{-1} K^{-1}) and T is the absolute temperature (K).

$$\ln K = \frac{\Delta S^\circ}{R} + \left(\frac{\Delta H^\circ}{RT}\right) \tag{10}$$

The slope and intercept of the plot of $\ln K$ vs. $1/T$ could be used to calculate the values of ΔH° and ΔS°, respectively, as shown in Fig. 9. The calculated values are given in Table 2. The enthalpy change ΔH° for the adsorption process shows a negative value, which reflects the exothermic nature of the adsorption. The randomness of the solid-solution interface of the SrOx-NPs adsorbent toward EBT is viewed from the positive entropy value. The negative values of free energy change reflect the adsorption reaction's spontaneous nature and thermodynamic feasibility [36].

Table 2
Thermodynamic parameters for removal of EBT using SrOx-NPs

T (K)	ΔG°, kJ mol^{-1}	ΔH°, kJ mol^{-1}	ΔS°, J mol^{-1} K^{-1}
298	−4.963		
308	−4.290		
318	−3.705	−25.494.13	68.972944
328	−2.800		
338	−2.264		

Table 3 compares the adsorption capacity of SrOx-NPs with some previously reported adsorbents of EBT. As shown, SrC$_2$O$_4$·2H$_2$O shows good adsorption capacity when compared with other adsorbents of EBT dye. The advantages of the adsorbent here are that the preparation method is easy and conventional (i.e., simple precipitation, filtration, and drying) and can be safely used in wastewater treatments. Moreover, the structure contains oxygen atoms in both oxalate group and water molecules, as well as hydrogen atoms in water molecules, which can easily bind to EBT molecules through hydrogen bonds.

Table 3
Comparison of the adsorption capacity of SrOx-NPs with other adsorbents of EBT

| No	Adsorbent	Adsorption capacity (mg g^{-1})	References
1	NiFe$_2$O$_4$ magnetic NPs	47.0	[37]
2	Activated charcoal	4.71	[38]
3	Magnetite/silica/pectin NPs	65.35	[39]
4	Untreated almond shell	6.02	[40]
5	Iron oxide nanoparticles	67.1	[41]
6	Tunisian almond shell	32.16	[42]
7	Sludge-derived activated carbon	178.2	[43]
8	Activated carbon prepared from waste rice hulls	2.021	[44]
9	[SrC$_2$O$_4$·2H$_2$O]-NPs	63.0	This work
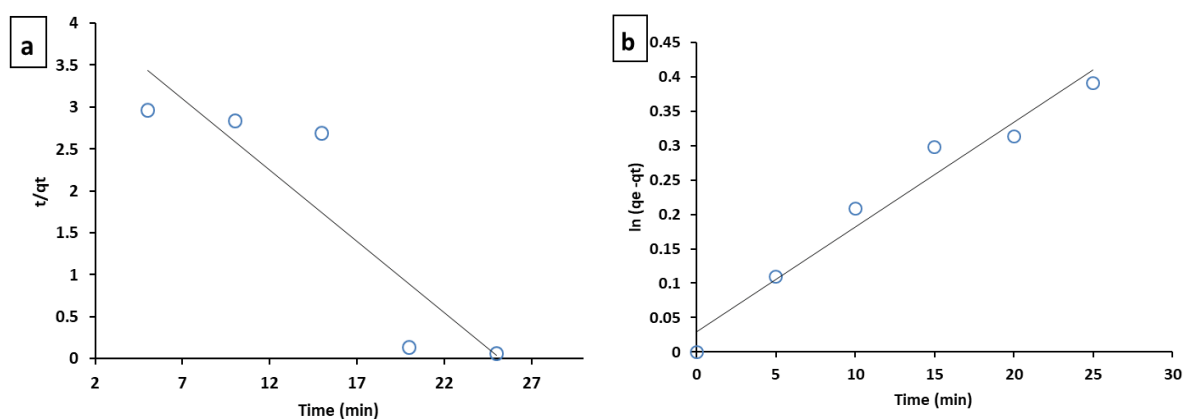
Fig. 8. Plots of pseudo-first-order (a) and pseudo-second-order (b) kinetic models for the adsorption of EBT with SrOx-NPs.
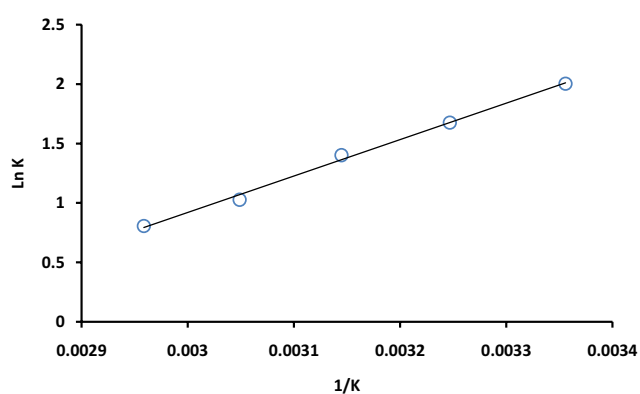

Fig. 9. Plot of ln$K$ against 1/T for removal of EBT on SrOx-NPs.

3.2.8. Adsorption mechanism

The mechanism of EBT adsorption on SrOx-NPs was evaluated by FT-IR spectra of SrOx-NPs, EBT, and EBT@SrOx-NPs. The spectrum of EBT@SrOx-NPs showed very low intensities of characteristic bands at 3,350 and 1,703 cm^{-1} when compared with the free SrOx-NPs spectrum, which suggests the participation of H$_2$O and COO, respectively, in the adsorption reaction. Also, the spectrum displayed the weakness of band at 3,458 cm^{-1}, which exists in the spectrum of EBT as a wide band indicates the involvement of the OH group in EBT in the adsorption process. These findings suggest the adsorption of EBT on SrOx-NPs via hydrogen bonding, Fig. 10.

4. Conclusion

In the present study, for the first time, nanoplates of Diaqua oxalato strontium(II) were used as an adsorbent for the removal of EBT in aqueous solution. Batch experiments were carried out to study the effects of different operational parameters such as dose amounts, contact time, initial dye concentrations, pH, and temperature on the adsorption process. The adsorption capacity of EBT was 63 mg g^{-1} under ideal conditions. The adsorption isotherm was studied using the Langmuir and Freundlich forms, and the results showed good agreement with the Freundlich form, which indicates the heterogeneous adsorption process. The kinetic adsorption mechanism was evaluated by applying the experimental data to pseudo-first-order and pseudo-second-order kinetic models. The results exhibited good fitting with the pseudo-second-order model. The adsorption mechanism was evaluated from experimental and spectral data, which can be explained as the binding of EBT with SrOx-NPs via hydrogen bonding.
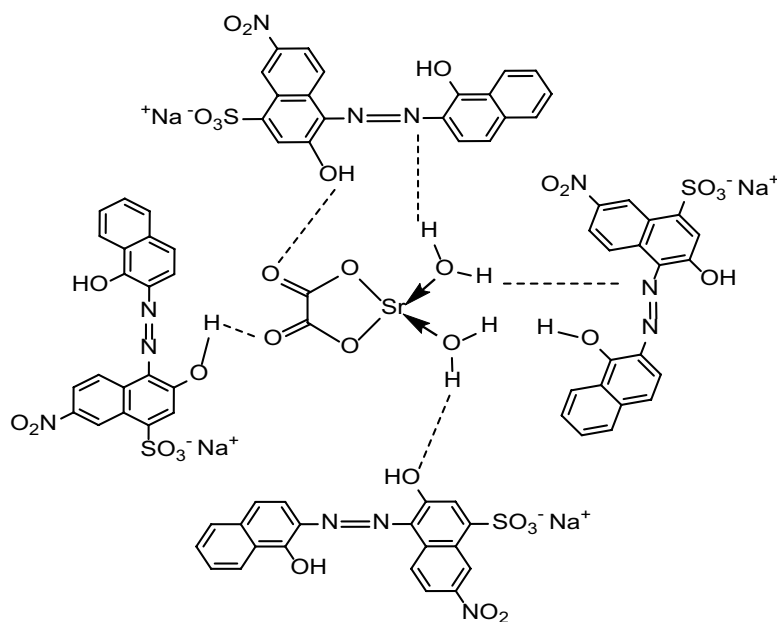
Fig. 10. Mechanism of EBT adsorption on SrOx-NPs.

Conflict of interest

None

Acknowledgment

References

[1] A.A. Essawy, A.M. Nassar, W.A.A. Arafa, A novel photocatalytic system consists of Co(II) complex@ZnO exhibits potent antimicrobial activity and efficient solar-induced wastewater remediation, Sol. Energy, 170 (2018) 388–397.

[2] I.H. Alsohaimi, A.M. Nassar, T.A.S. Elnasr, B.A. Cheba, A novel composite silver nanoparticles loaded calcium oxide stemming from egg shell recycling: a potent photocatalytic and antibacterial activities, J. Cleaner Prod., 248 (2020) 119274, doi: 10.1016/j.jclepro.2019.119274.

[3] J. Kanagaraj, T. Senthilvelan, R.C. Panda, Degradation of azo dyes by laccase: biological method to reduce pollution load in dye wastewater, Clean Technol. Environ. Policy, 17 (2015) 1443–1456.

[4] A. Gottlieb, C. Shaw, A. Smith, A. Wheatley, S. Forsythe, The toxicity of textile reactive azo dyes after hydrolysis and decolourisation, J. Biotechnol., 101 (2003) 49–56.

[5] K.-T. Chung, Azo dyes and human health: a review, J. Environ. Sci. Health., Part C Environ. Carcinog. Ecotoxicol. Rev., 34 (2016) 233–261.

[6] S. Sohrabnezhad, S.D. Mooshangaie, In situ fabrication of n-type Ag/AgBr nanoparticles in MCM-41 with rice husk (RH/MCM-41) composite for the removal of Eriochrome Black T, Mater. Sci. Eng., B, 240 (2019) 16–22.

[7] A. Khalid, M. Zubair, Ihsanullah, A comparative study on the adsorption of Eriochrome Black T dye from aqueous solution on graphene and acid-modified graphene, Arabian J. Sci. Eng., 43 (2018) 2167–2179.

[8] M. Bansal, P.K. Patnala, T. Dugmore, Adsorption of Eriochrome Black T (EBT) using tea waste as a low cost adsorbent by batch studies: a green approach for dye effluent treatments, Curr. Res. Green Sustainable Chem., 3 (2020) 100036, doi: 10.1016/j.crgsc.2020.100036.

[9] M. Rabe, D. Verdes, S. Seeger, Understanding protein adsorption phenomena at solid surfaces, Adv. Colloid Interface Sci., 162 (2011) 87–106.

[10] G.A. Haghighat, S. Sadeghi, M.H. Saghi, S.K. Ghadiri, I. Anastopoulos, D.A. Giannakoudakis, J.C. Colmenares, M. Shams, Zeolitic imidazolate frameworks (ZIFs) of various morphologies against Eriochrome Black T (EBT): optimizing the key physicochemical features by process modeling, Colloids Surf., A, 606 (2020) 125391, doi: 10.1016/j.colsurfa.2020.125391.

[11] S. Sadeghi, H.R. Zakeri, M.H. Saghi, S.K. Ghadiri, S.S. Talebi, M. Shams, G.L. Dotto, Modified wheat straw–derived graphene for the removal of Eriochrome Black T: characterization, isotherm, and kinetic studies, Environ. Sci. Pollut. Res., 28 (2021) 3556–3556.

[12] M.D.G. de Luna, E.D. Flores, D.A.D. Genuino, C.M. Futalan, M.-W. Wan, Adsorption of Eriochrome Black T (EBT) dye using activated carbon prepared from waste rice hulls—optimization, isotherm and kinetic studies, J. Taiwan Inst. Chem. Eng., 44 (2013) 646–653.

[13] M. Zubair, N.D. Mu'azu, N. Jarrah, N.I. Blaisi, H.A. Aziz, M.A. Al-Harthi, Adsorption behavior and mechanism of Methylene Blue, Crystal Violet, Eriochrome Black T, and Methyl Orange Dyes onto biochar-derived date palm fronds waste produced at different pyrolysis conditions, Water, Air, Soil, Pollut., 231 (2020) 240, doi: 10.1007/s11270-020-04595-x.

[14] I. Khurana, A.K. Shaw, J.M. Khurana, P.K. Rai, Batch and dynamic adsorption of Eriochrome Black T from water on magnetic graphene oxide: experimental and theoretical studies, J. Environ. Chem. Eng., 6 (2018) 468–477.

[15] A. Deb, A. Debnath, B. Saha, Sono-assisted enhanced adsorption of Eriochrome Black T dye onto a novel polymeric nano-composite: kinetic, isotherm, and response surface methodology optimization, J. Dispersion Sci. Technol., 42 (2020) 1579–1592.

[16] A. Mittal, V.K. Gupta, Adsorptive removal and recovery of the azo dye Eriochrome Black T, Toxicol. Environ. Chem., 92 (2010) 1813–1823.

[17] M. Zoraga, C. Kahruman, I. Yusufoglu, Kinetics of celestite conversion to acidic strontium oxalate hydrate in aqueous solution of oxalic acid, Trans. Nonferrous Met. Soc. China, 29 (2019) 1332–1345.

[18] G. Vanhoyland, F. Bourée, M.K. Van Bael, J. Mullens, L.C. Van Poucke, Structure determination and refinement of acid strontium oxalate from X-ray and neutron powder diffraction, J. Solid State Chem., 157 (2001) 283–288.

[19] A.M. Nassar, A.M. Elseman, I.H. Alsohaimi, N.F. Alotaibi, A. Khan, Diaqua oxalato strontium(II) complex as a precursor for facile fabrication of Ag-NPs@SrCO$_3$, characterization, optical properties, morphological studies and adsorption efficiency, J. Coord. Chem., 72 (2019) 771–785.

[20] T.-Z. Ren, X.-H. Zhu, T.-Y. Ma, Z.-Y. Yuan, Adsorption of methylene blue from aqueous solution by periodic mesoporous titanium phosphonate materials, Adsorpt. Sci. Technol., 31 (2013) 535–548.

[21] Y. Chen, S. Li, Q.S. Wu, Simultaneous synthesis of strontium oxalate with different morphology by living bi-template, J. Exp. Nanosci., 10 (2015) 268–273.

[22] E.A. Zeid, A.M. Nassar, M.A. Hussein, M.M. Alam, A.M. Asiri, H.H. Hegazy, M.M. Rahman, Mixed oxides CuO-NiO fabricated for selective detection of 2-Aminophenol by electrochemical approach, J. Mater. Res. Technol., 9 (2020) 1457–1467.

[23] A.M. Nassar, A.M. Hassan, S.S. Alabd, Antitumor and antimicrobial activities of novel palladacycles with abnormal aliphatic CH activation of Schiff Base 2-[(3-phenylallylidene) amino] phenol, Synth. React. Inorg. Met.-Org. Chem., 45 (2015) 256–270.

[24] A.M. Nassar, E.A. Zeid, A.M. Elseman, N.F. Alotaibi, A novel heterometallic compound for design and study of electrical properties of silver nanoparticles-decorated lead compounds, New J. Chem., 42 (2018) 1387–1395.

[25] A.M. Nassar, Catalytic reactivity of new Ni(II), Cu(II) and Sn(II) complexes for decolorization of indigo carmine in aqueous solution, high efficiency of copper complex, Appl. Organomet. Chem., 32 (2018) e4056.

[26] A.M. Elseman, A.E. Shalan, M.M. Rashad, A.M. Hassan, N.M. Ibrahim, A.M. Nassar, Easily attainable new approach to mass yield ferrocenyl Schiff base and different metal complexes of ferrocenyl Schiff base through convenient ultrasonication-solvothermal method, J. Phys. Org. Chem., 30 (2017) e3639.

[27] A.M. Nassar, A.M. Hassan, A.N. Elkmash, Synthesis, characterization, corrosion inhibition of mild steel in HCl (0.5 N) solution and solid-state electrical conductivity of new Co(II), Ni(II), Cu(II) and Zn(II) complexes, Appl. Organomet. Chem., 31 (2017) e3572.

[28] E. Bazrafshan, F.K. Mostafapour, A.R. Hosseini, A. Raksh Khorshid, A.H. Mahvi, Decolorisation of Reactive Red 120 dye by using single-walled carbon nanotubes in aqueous solutions, J. Chem., 2013 (2013) 938374, doi: 10.1155/2013/938374.

[29] M. Zubair, N. Jarrah, M.S. Manzar, M. Al-Harthi, M. Daud, N.D. Mu'azu, S.A. Haladu, Adsorption of Eriochrome Black T from aqueous phase on MgAl-, CoAl- and NiFe-calcined layered double hydroxides: kinetic, equilibrium and thermodynamic studies, J. Mol. Liq., 230 (2017) 344–352.

[30] S. Akhouairi, H. Ouachtak, A.A. Addi, A. Jada, J. Douch, Natural sawdust as adsorbent for the Eriochrome Black T dye removal from aqueous solution, Water, Air, Soil, Pollut., 230 (2019) 181, doi: 10.1007/s11270-019-4234-6.

[31] A. Khalid, M. Zubair, A comparative study on the adsorption of Eriochrome Black T dye from aqueous solution on graphene and acid-modified graphene, Arabian J. Sci. Eng., 43 (2018) 2167–2179.

[32] P. Shanmugam, W. Wei, K. Qian, Z. Jiang, J. Lu, J. Xie, Efficient removal of Erichrome Black T with biomass-derived magnetic carbonaceous aerogel sponge, Mater. Sci. Eng., B, 248 (2019) 114387, doi: 10.1016/j.mseb.2019.114387.

[33] T.S. Khayyun, A.H. Mseer, Comparison of the experimental results with the Langmuir and Freundlich models for copper removal on limestone adsorbent, Appl. Water Sci., 9 (2019) 170, doi: 10.1007/s13201-019-1061-2.

[34] J.P. Simonin, On the comparison of pseudo-first-order and pseudo-second-order rate laws in the modeling of adsorption kinetics, Chem. Eng. J., 300 (2016) 254–263.

[35] N. Mohammadi, H. Khani, V.K. Gupta, E. Amereh, S. Agarwal, Adsorption process of methyl orange dye onto mesoporous carbon material–kinetic and thermodynamic studies, J. Colloid Interface Sci., 362 (2011) 457–462.

[36] S.M. Al-Rashed, A.A. Al-Gaid, Kinetic and thermodynamic studies on the adsorption behavior of Rhodamine B dye on Duolite C-20 resin, J. Saudi Chem. Soc., 16 (2012) 209–215.

[37] F. Moeinpour, A. Alimoradi, M. Kazemi, Efficient removal of Eriochrome Black T from aqueous solution using NiFe$_2$O$_4$ magnetic nanoparticles, J. Environ. Health. Sci. Eng., 12 (2014) 112, doi: 10.1186/s40201-014-0112-8.

[38] M.J. Iqbal, M.N. Ashiq, Adsorption of dyes from aqueous solutions on activated charcoal, J. Hazard. Mater., 139 (2007) 57–66.

[39] O.A. Attallah, M.A. Al-Ghobashy, M. Nebsen, M.Y. Salem, Removal of cationic and anionic dyes from aqueous solution with magnetite/pectin and magnetite/silica/pectin hybrid nanocomposites: kinetic, isotherm and mechanism analysis, RSC Adv., 6 (2016) 11461–11480.

[40] O. Şahin, C. Saka, S. Kutluay, Cold plasma and microwave radiation applications on almond shell surface and its effects on the adsorption of Eriochrome Black T, J. Ind. Eng. Chem., 19 (2013) 1617–1623.

[41] B. Saha, S. Das, J. Saikia, G. Das, Preferential and enhanced adsorption of different dyes on iron oxide nanoparticles: a comparative study, J. Phys. Chem. C, 115 (2011) 8024–8033.

[42] R.B. Arfi, S. Karoui, K. Mougin, A. Ghorbal, Adsorptive removal of cationic and anionic dyes from aqueous solution by utilizing almond shell as bioadsorbent, Euro-Med. J. Environ. Integr., 2 (2017) 20, doi: 10.1007/s41207-017-0032-y.

[43] H. Wen, D. Zhang, L. Gu, H. Yu, M. Pan, Y. Huang, Preparation of sludge-derived activated carbon by fenton activation and the adsorption of Eriochrome Black T, Materials, 12 (2019) 882, doi: 10.3390/ma12060882.

[44] M.D.G. de Luna, E.D. Flores, D.A.D. Genuino, C.M. Futalan, M.W. Wan, Adsorption of Eriochrome Black T (EBT) dye using activated carbon prepared from waste rice hulls—optimization, isotherm and kinetic studies, J. Taiwan Inst. Chem. Eng., 44 (2013) 646–653.